ISSN 1674-1056
http://cpb.iphy.ac.cn
http://iopscience.iop.org/cpb
中国物理 B
Chinese Physics
中国物理 Chinese Physics B

Aperture efficiency and mode constituent analysis for OAM vortex beam generated by digital metasurface

Di Zhang(张迪), Xiangyu Cao(曹祥玉), Huanhuan Yang(杨欢欢), Jun Gao(高军), Shiqi Lv(吕世奇)

Citation: Chin. Phys. B . 2019, 28(3): 034204. **doi:** 10.1088/1674-1056/28/3/034204
Journal homepage: http://cpb.iphy.ac.cn; http://iopscience.iop.org/cpb

What follows is a list of articles you may be interested in

Total ionizing dose effects in pinned photodiode complementary metal-oxide-semiconductor transistor active pixel sensor

Lin-Dong Ma(马林东), Yu-Dong Li(李豫东), Lin Wen(文林), Jie Feng(冯婕), Xiang Zhang(张翔), Tian-Hui Wang(王田珲), Yu-Long Cai(蔡毓龙), Zhi-Ming Wang(王志铭), Qi Guo(郭旗)

Chin. Phys. B . 2018, 27(10): 104207. **doi:** 10.1088/1674-1056/27/10/104207

A new method of calculating the orbital angular momentum spectra of Laguerre-Gaussian beams in channels with atmospheric turbulence

Xiao-zhou Cui(崔小舟), Xiao-li Yin(尹霄丽), Huan Chang(常欢), Zhi-chao Zhang(张志超), Yong-jun Wang(王拥军), Guo-hua Wu(吴国华)

Chin. Phys. B . 2017, 26(11): 114207. **doi:** 10.1088/1674-1056/26/11/114207

Orbital angular momentum density and spiral spectra of Lorentz-Gauss vortex beams passing through a single slit

Zhi-Yue Ji(季志跃), Guo-Quan Zhou(周国泉)

Chin. Phys. B . 2017, 26(9): 094202. **doi:** 10.1088/1674-1056/26/9/094202

Microscale vortex laser with controlled topological charge

Xing-Yuan Wang(王兴远), Hua-Zhou Chen(陈华洲), Ying Li(黎颖), Bo Li(李波), Ren-Min Ma(马仁敏)

Chin. Phys. B . 2016, 25(12): 124211. **doi:** 10.1088/1674-1056/25/12/124211

Turbulence mitigation scheme based on multiple-user detection in an orbital-angular-momentum multiplexed system

Li Zou(邹丽), Le Wang(王乐), Sheng-Mei Zhao(赵生妹), Han-Wu Chen(陈汉武)

Chin. Phys. B . 2016, 25(11): 114215. **doi:** 10.1088/1674-1056/25/11/114215

Aperture efficiency and mode constituent analysis for OAM vortex beam generated by digital metasurface

Di Zhang(张迪), Xiangyu Cao(曹祥玉)†, Huanhuan Yang(杨欢欢), Jun Gao(高军), and Shiqi Lv(吕世奇)

Air Force Engineering University, Xi'an 710077, *China*

(Received 19 November 2018; revised manuscript received 22 December 2018; published online 25 February 2019)

A systematic study of the aperture efficiency and mode constituent for orbital angular momentum (OAM) vortex beam generated by digital metasurface is presented. The aperture efficiency and OAM spectrum are computed for different bit numbers. It is found that the aperture efficiency declines for digital metasurface due to the phase quantization error, especially for 1-bit device. Fortunately, the OAM spectrum is barely affected by phase quantization and the designated main mode keeps dominant for different bit numbers, indicating that high purity OAM vortex beam can be generated by digital metasurface. Besides, the influence of topological charge l is also investigated. For a fixed metasurface, the radiation performance deteriorates sharply with the growing of l and the parasitic OAM mode becomes dominant at certain angle. At last, a prototype of 1-bit metasurface was simulated, fabricated and measured in anechoic chamber. The simulation and experiment results verify the correctness of the numerical analysis.

Keywords: orbital angular momentum (OAM), efficiency, mode constituent, metasurface

PACS: 42.50.Tx, 42.79.Ag **DOI:** 10.1088/1674-1056/28/3/034204

1. Introduction

Orbital angular momentum (OAM) was discovered in light beams in 1992 for the first time.[1] Since then, OAM vortex beam has attracted tremendous interests.[2–7] At the very beginning, the research of OAM mainly focused on optics field. Until 2007, the concept of photon OAM was extended to microwave bands and a simulation was conducted to generate OAM vortex beam utilizing phased array antenna.[8] In 2012, an experiment successfully demonstrated that the OAM vortex beam can be utilized to increase wireless communication capacity,[9] which is an inspiring achievement for the scarce spectrum resource. Besides, the OAM vortex beam can also be applied to other fields such as radar pulse generation[10] and radar targets detection,[11] naming a few. Therefore, the research of OAM vortex beam in microwave bands is of great significance. The standard OAM generation approach includes spiral phase plate (SPP),[12] holographic plate,[13] circular traveling-wave antenna[14] and so on. Quite recently, a novel method was proposed to generate OAM vortex radio beams utilizing a reflective metasurface.[15] By carefully tailoring the reflection phase of each element constituting the metasurface, the helical phase profile related with $e^{il\varphi}$ can be obtained. Due to the powerful manipulation ability on electromagnetic waves, metasurface was widely applied to the generation of OAM vortex radio beams in the following researches.[16–21] Designing the elements that can provide 2π phase shift is the challenge for such metasurfaces. In fact, a more concise device called digital metasurface has been applied to antenna designs since the concept was proposed in 2014.[22] The elements of n-bit digital metasurface have 2^n discrete reflection/transmission phase states[23] and do not need to cover the whole 2π phase range. These elements can be coded into different sequences to obtain different desired functions.[24] Moreover, the reconfigurable designs for reflectarray antennas can also be realized by using digital metasurface.[25] In the previous research, we have successfully introduced the digital metasurface into the generation of OAM vortex beam.[26] Nevertheless, there still exist two important issues which are worthy of being studied. One is the aperture efficiency, which is a non-ignorable index in metasurface applications especially for digital metasurface devices. The other one is the mode constituent of the OAM vortex beam, which directly indicates the mode purity of the generated OAM vortex beam.

In this paper, the quantitative analysis of the aperture efficiency and mode constituent for OAM vortex beam generated by digital metasurface is carried out. The mathematical modeling for OAM vortex beam generation is presented first. Afterwards, the numerical computation based on the mathematical model is conducted for different bit numbers and topological charges. Then, a 1-bit metasurface is simulated, fabricated and experimentally measured to demonstrate the numerical computation. In the end, conclusions are drawn to summarize the work of this paper.

2. Mathematical modeling

Consider a metasurface composed of $M \times N$ elements. It is illuminated by the incident wave irradiated from a feeding horn antenna, which is located above the center of the meta-

†Corresponding author. E-mail: xiangyucaokdy@163.com

© 2019 Chinese Physical Society and IOP Publishing Ltd

surface as shown in Fig. 1. The reflected wave is given by[27]

$$E(\theta,\varphi)=\cos^{q_e}\theta\sum_{m=1}^{M}\sum_{n=1}^{N}A_{mn}\,\mathrm{e}^{-\mathrm{j}kr_{\mathrm{f}mn}}\,\mathrm{e}^{\mathrm{j}\varphi_{mn}}\,\mathrm{e}^{\mathrm{j}k\boldsymbol{r}_{mn}\cdot\boldsymbol{u}},\quad(1)$$

where

$$A_{mn}=\frac{\cos^{q_f}\theta_{\mathrm{f}mn}\cos^{q_e}\theta_{emn}\,|\Gamma_{mn}|}{r_{\mathrm{f}mn}}.\quad(2)$$

Here, $\cos^{q_e}\theta$ is the element pattern in transmission mode and q_e is 1 unless otherwise specified. $kr_{\mathrm{f}mn}$ is the phase introduced by the different incident path. φ_{mn} and $\boldsymbol{r}_{mn}$ are the compensated phase and position vector of the mn^{th} element, respectively. $\boldsymbol{u}$ is the unit vector of arbitrary direction. $\cos^{q_f}\theta_{\mathrm{f}mn}$ is the feeding pattern of the horn antenna and $\cos^{q_e}\theta_{emn}$ is the element pattern in receiving mode. q_f is set to be 6.5 to simulate the radiation pattern of the feeding horn. $|\Gamma_{mn}|$ represents the reflection magnitude of the mn^{th} element and is assumed to be 1. k is the wavenumber in vacuum. The angles, vectors, and distances are depicted in Fig. 1. In order to generate OAM vortex beam in $\boldsymbol{u}$ direction, the compensated phase φ_{mn} is supposed to satisfy

$$-kr_{\mathrm{f}mn}+\varphi_{mn}+k\boldsymbol{r}_{mn}\cdot\boldsymbol{u}|_{u=u_0}=l\Phi_{mn},\quad(3)$$

with l being the topological charge of OAM and Φ_{mn} the azimuthal angle of the mn^{th} element.

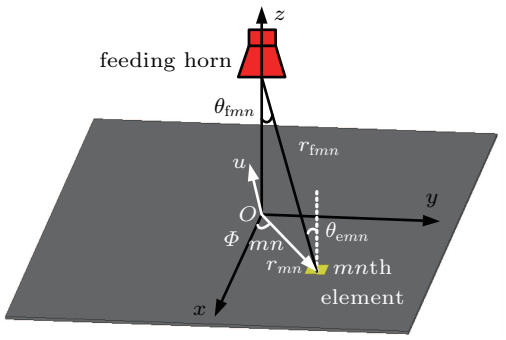


Fig. 1. Schematic illustration of the reflectarray antenna. O is the center point of the metasurface.

Figure 2(a) gives the distribution map of φ_{mn} at 6 GHz for generation of OAM vortex beam in normal direction. Note that the element size is 15 mm× 15 mm and the scale of the metasurface is 30×30. Besides, the distance between the feeding horn antenna and the reflective metasurface is 400 mm. The normalized radiation pattern and phase distribution in uv plane ($u=\sin\theta\cos\varphi$, $v=\sin\theta\sin\varphi$) are respectively shown in Figs. 2(b) and 2(c). The doughnut-like main lobe and phase related with azimuthal angle can be clearly observed, indicating that OAM vortex beam is successfully generated.

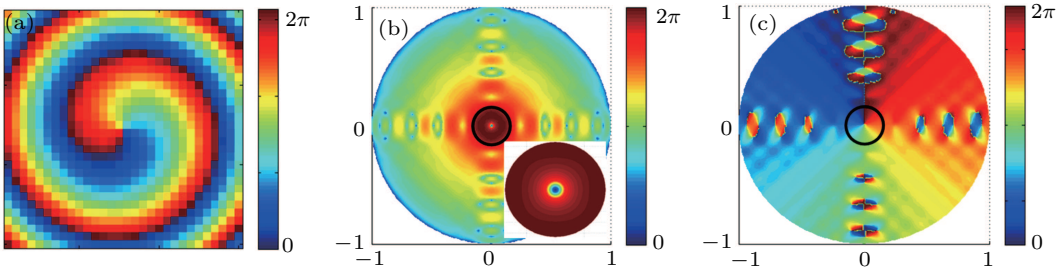


Fig. 2. (a) The compensated phase of the elements across the metasurface. (b) and (c) are the radiation pattern and phase distribution in uv plane, respectively. The black circles in panels (b) and (c) denote the main lobe and the inset at lower right corner of panel (b) is the megascopic main lobe.

Phase quantization is the main characteristic of digital metasurface. For n-bit ($n=1, 2, 3, \ldots$) phase quantization, the compensated phase $\varphi_{mn}|_{n\text{-bit}}$ is given by

$$\varphi_{mn}|_{n-\mathrm{bit}}=\begin{cases}\pi/2^n, & 0\le\varphi_{mn}<2\pi/2^n,\\ \pi/2^n+1\cdot(2\pi/2^n), & 2\pi/2^n\le\varphi_{mn}<2\cdot(2\pi/2^n),\\ \vdots & \\ \pi/2^n+(2^n-1)\cdot(2\pi/2^n), & (2^n-1)\cdot(2\pi/2^n)\le\varphi_{mn}\le2\pi.\end{cases}\quad(4)$$

Figures 3(a), 3(b), and 3(c) are the 1-bit, 2-bit, and 3-bit compensated phase transformed from the continuous phase φ_{mn} shown in Fig. 2(a), respectively. The corresponding radiation patterns and phase distributions in the uv plane are depicted in Figs. 3(d)–3(i). It is seen that OAM vortex beams are all successfully generated by 1-bit, 2-bit, and 3-bit digital metasurface.

3. Aperture efficiency and mode constituent analysis

Due to the existence of phase quantization error,[23] the radiation performance of digital reflectarray antennas are worsened at different levels, which can be seen from Figs. 3(d), 3(e), and 3(f). Thus, it is of high necessity to analyze the aperture efficiency and mode constituent for OAM vortex beam.

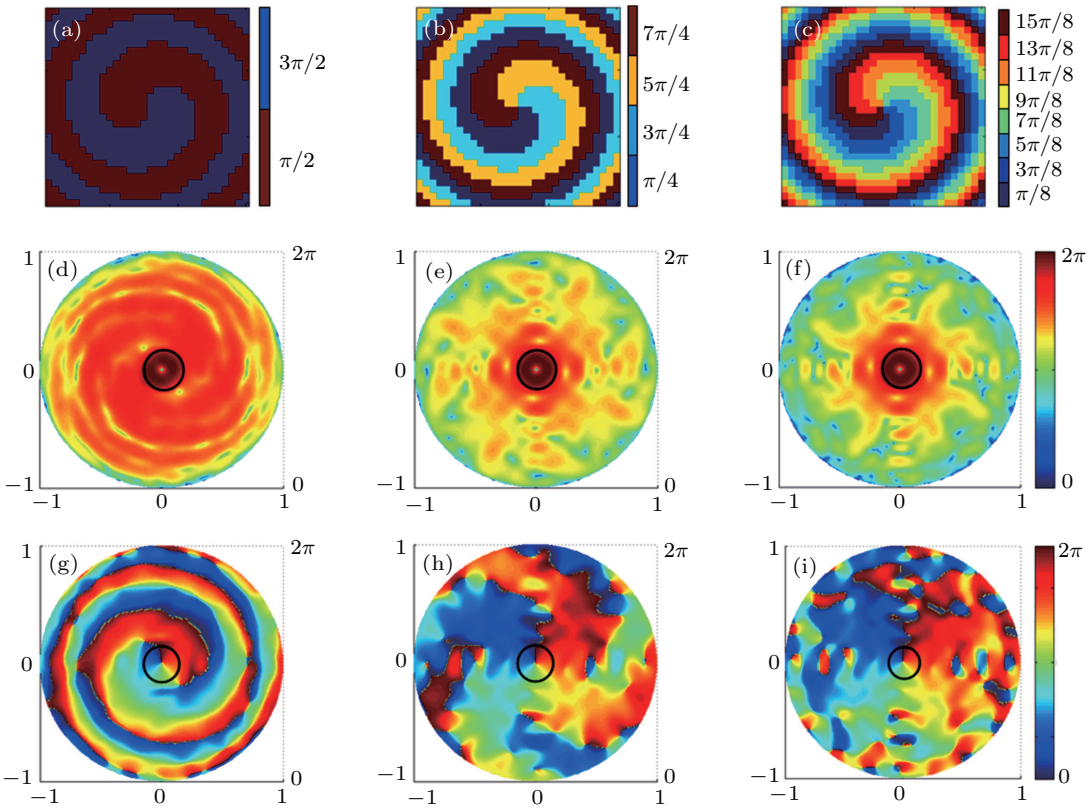


Fig. 3. (a)–(c) The compensated phase for 1-bit, 2-bit, and 3-bit metasurface, respectively. (d)–(f) Corresponding radiation patterns. (g)–(i) Corresponding phase distributions.

Table 1. Gain and aperture efficiency for different metasurfaces.

Metasurface	Peak gain/dB	Aperture efficiency
Continuous	21.7	14.6%
1-bit	19.4	8.5%
2-bit	21.5	14.0%
3-bit	21.6	14.5%
Ref. [28]	19.9(X band), 18.8(C band)	7.1%(X band), 13.8%(C band)
Ref. [29]	21.5	12.09%

The gain value versus θ in $\varphi = 0$ plane is shown in Fig. 4(a). Obvious gain loss and strengthened side lobes can be observed for 1-bit pattern compared with the continuous one, which is caused by the large quantization error. While for 2-bit and 3-bit metasurfaces, the quantization error is much smaller than 1-bit design so that the corresponding radiation patterns agree well with that of the continuous one. Table 1 lists the peak gain values in full space and the aperture efficiency η given by

$$\eta = \frac{G}{4\pi A/\lambda^2}, \tag{5}$$

where G is the peak gain, A represents the aperture size of the metasurface, and λ denotes the working wavelength in free space. It is seen in Table 1 that the peak gain of 1-bit metasurface is 2.3 dB lower than that of the continuous one, making the aperture efficiency drop from 14.6% to 8.5%. For 2-bit and 3-bit metasurface, the gain loss is rather small and the aperture efficiency is quite close to the continuous one. It is worth mentioning that the aperture efficiency of the proposed metasurface is comparable with other works.[28,29]

The OAM spectrum is the complex Fourier transform of the OAM vortex beam. Their numerical relationship is given by[30]

$$A_l = \frac{1}{2\pi}\int_0^{2\pi} \psi(\varphi)\,\mathrm{d}\varphi\, \mathrm{e}^{-\mathrm{j}l\varphi}, \tag{6}$$

$$\psi(\varphi) = \sum_l A_l\, \mathrm{e}^{\mathrm{j}l\varphi}, \tag{7}$$

where $\psi(\varphi)$ is the phase value extracted along the sampling circle centered on the beam axis. In this paper, a circle containing the maximum field (black circles in Fig. 3) is chosen as the sampling circle. It is worth mentioning that the bit number does not affect the size of the sampling circle because it has no relationship with the divergence angle of the OAM vortex beam.[31] Figure 4(b) gives the OAM spectrum of the vortex beams with topological charge $l = 1$ generated by different metasurfaces. $\psi(\varphi)$ is extracted at $\theta = 5°$. It is seen that the OAM mode with $l = 1$ is dominant for all metasurfaces as expected. The parasitic modes with $l = -3$ and $l = 5$ are also observed, but they are extremely small. Especially, for 1-bit metasurface, the parasitic modes are also stimulated at $l = -1$ and $l = 3$. Nevertheless, these parasitic modes are still small enough to be neglected. Thus, a meaningful conclusion can be drawn that high purity OAM vortex beam can be generated by digital metasurface, including the 1-bit device which has the largest quantization error.

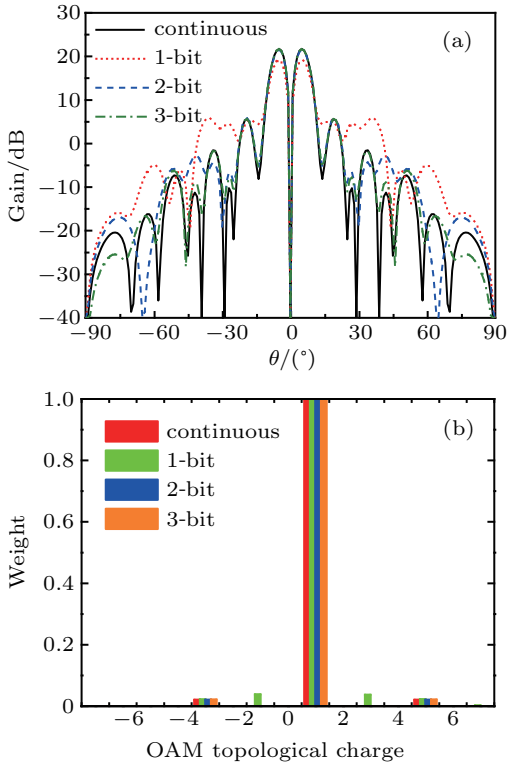


Fig. 4. (a) The radiation patterns in $\varphi = 0$ plane and (b) the OAM spectrum of vortex beam generated by different metasurfaces.

For a fixed metasurface, the radiation performance of OAM vortex beam is closely related with topological charge l. Figures 5(a) and 5(b) depict the radiation patterns in $\varphi = 0$ plane of OAM vortex beam with $l = 3$ and $l = 5$. It is apparent that the gain is sharply reduced compared with that of $l = 1$. Besides, the enlarged divergence angle and enhanced side lobes are also observed. Table 2 lists the corresponding peak gain values in full space and aperture efficiency for $l = 3$ and $l = 5$, respectively. With the increase of l, the radiation performance deteriorates rapidly. For $l = 5$, the maximum gain drops to 14.7 dB and the aperture efficiency falls to 2.9% for the continuous metasurface. These two indexes are even lower for 1-bit metasurface. This phenomenon indicates that for a fixed metasurface, overlarge topological charge l is inadvisable in practical applications.

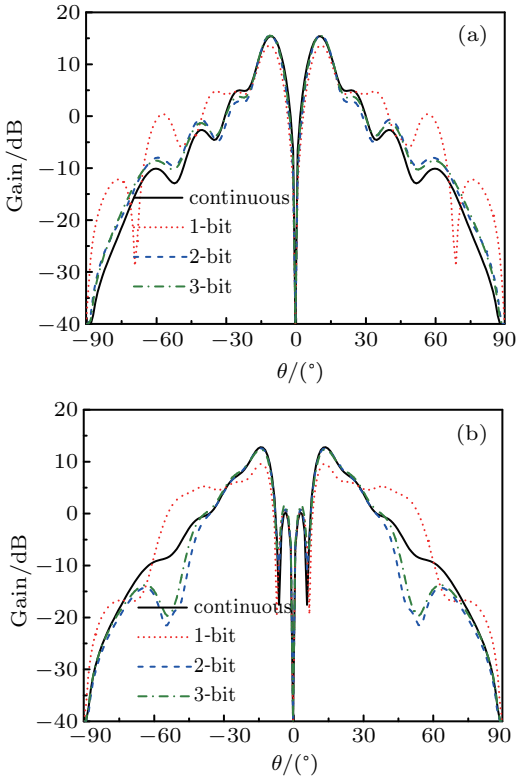


Fig. 5. The radiation patterns of OAM vortex beam in $\varphi = 0$ plane with (a) $l = 3$ and (b) $l = 5$.

Table 2. Gain and aperture efficiency for $l = 3$ and $l = 5$.

Metasurface	Peak gain/dB		Aperture efficiency	
	$l = 3$	$l = 5$	$l = 3$	$l = 5$
Continuous	17.1	14.7	5%	2.9%
1-bit	14.8	12.3	2.9%	1.7%
2-bit	17.0	14.5	4.9%	2.8%
3-bit	17.1	14.7	5%	2.9%

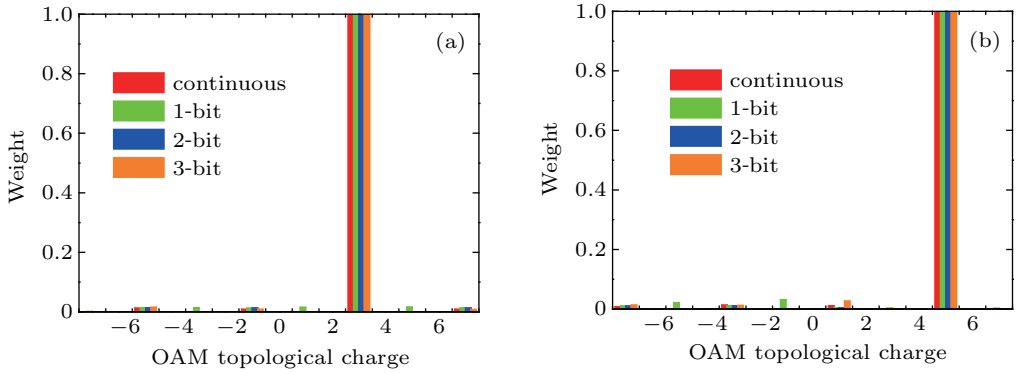


Fig. 6. The spectrums of OAM vortex beam plane with (a) $l = 3$ and (b) $l = 5$.

Next, the OAM mode constituent is discussed. Figure 6 shows the spectrum of OAM vortex beam with $l = 3$ and $l = 5$. $\psi(\varphi)$ is extracted at $\theta = 11°$ for $l = 3$ and $\theta = 14°$ for $l = 5$, both denoting the direction of maximum radiation. Different from the deterioration of radiation pattern, the designated mode is still dominant in the domain of main lobe. The other

parasitic modes can also be neglected. Nevertheless, a parasitic beam, which is very similar to OAM vortex beam, is observed between the two radiation peaks of the main lobe for $l = 5$ shown in Fig. 5(b). It is quite necessary to analyze the constituent of this parasitic beam. Thus, $\psi(\varphi)$ is extracted at $\theta = 3^\circ$ (the peak direction of the parasitic beam) to compute the spectrum, which is shown in Fig. 7. A dominant mode of $l = 1$ is observed for all the metasurfaces. Besides, the other modes of $l = -3$ and $l = 5$ are also seen but are quite small. Specially, two other larger parasitic modes occur at $l = -1$ and $l = 3$ for 1-bit metasurface, which is in good agreement with that of the designated $l = 1$ vortex beam shown in Fig. 4(b). The OAM spectrum manifests that the parasitic beam is indeed the OAM vortex beam. This vortex beam may be generated when the designated main mode l is overlarge. To eliminate the parasitic beam, we can enlarge the scale of the metasurface.

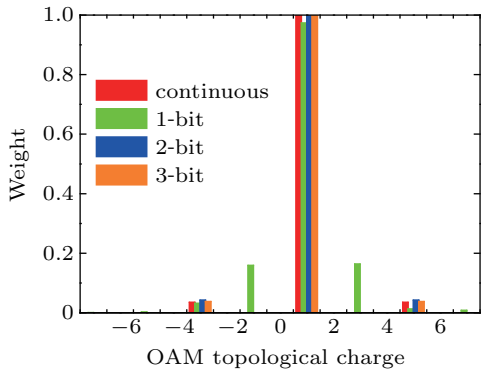


Fig. 7. The OAM spectrum of the parasitic beam between the two peaks of $l = 5$ vortex beam.

4. Prototype test

To verify the computations, a prototype of the 1-bit metasurface was simulated, fabricated and measured in anechoic chamber. Note that the topological charge of the generated OAM vortex beam was $l = 1$. The metasurface is composed of two kinds of elements as shown in Figs. 8(a) and 8(b). These elements were metallic patches etched on substrate ($\varepsilon_r = 2.65$) with a metallic ground. The thickness of the substrate is 3 mm. Figure 8(c) depicts the simulated reflection phase of the elements versus frequency. The simulation was conducted using commercial software HFSS. It is seen that the reflection phase difference of the two kinds of elements is π at 6 GHz, satisfying the condition of 1-bit phase quantization. According to the compensated phase distribution shown in Fig. 3(a), the 1-bit metasurface is configured as shown in Fig. 8(d). By using PCB (Printed Circuit Board) technology, a prototype was fabricated and measured in anechoic chamber. A standard horn working at 6 GHz was used as the feeding antenna as shown in Fig. 8(e). A tailor-made structure was employed to hold the metasurface and the feeding horn. In the experiment, vertical polarization was employed. It is worth mentioning that horizontal polarization is also effective since the reflection phase of the elements keeps the same under both polarizations.

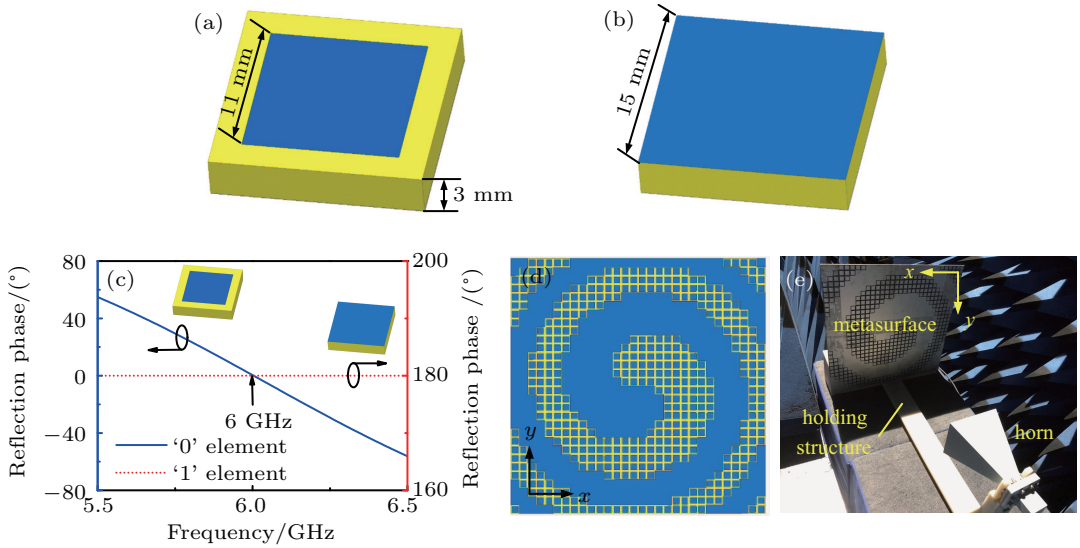


Fig. 8. (a), (b) The elements with 0 reflection phase and π reflection phase, respectively. (c) The reflection phase versus frequency for the two kinds of elements. (d) The configuration of the 1-bit metasurface. (e) The fabricated metasurface, feed horn, and the holding structure.

The radiation phase distribution on observation plane was measured and shown in Fig. 9. For contrast, the simulated result is also depicted. The observation plane with the size of 1000 mm× 1000 mm is parallel to the metasurface aperture and the distance between them is 3 m. It is seen that the helical phase front was obtained. The measured result agrees well with the simulated one. The radiation patterns and OAM mode spectrum obtained through numerical computation, HFSS simulation and experiment test are depicted in Fig. 10(a). The measured side lobes are higher than that

of the numerical and HFSS result, which is due to the fabrication error and measurement error. In general, however, the measurement result agrees well with the other two. Table 3 lists the comparison of the corresponding gain and efficiency. It is observed that the gains of HFSS and experiment results are approximately 1 dB and 2.2 dB lower than the numerical one, respectively, making the aperture efficiency decrease by about 1.7% and 3.3%. This reduction is mainly attributed to the blockage effect of the feeding horn, which does not exist in numerical computation. On the other hand, according to the OAM spectrum shown in Fig. 10(b), it is found that the $l = 1$ mode of the HFSS and experiment results is slightly lower than numerical one, but is still dominant. The other parasitic modes are much smaller. Generally, the HFSS and experiment results agree well with the numerical computations, verifying the correctness of the analysis.

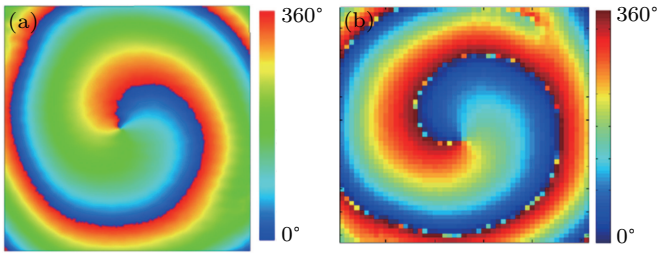


Fig. 9. (a) Simulated and (b) measured phase distribution on the observation plane.

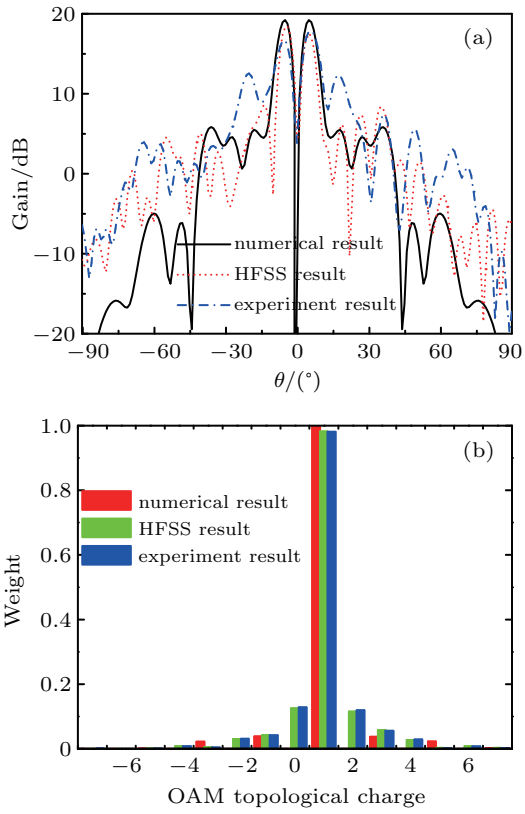


Fig. 10. (a) Radiation patterns in $\varphi = 0$ plane and (b) OAM spectrum of vortex beam generated by 1-bit metasurface.

Table 3. Comparison of gain and aperture efficiency for 1-bit metasurface.

Metasurface	Peak gain/dB	Aperture efficiency
Numerical	19.4	8.5%
HFSS	18.4	6.8%
Experiment	17.2	5.2%

5. Conclusion

In summary, the aperture efficiency and mode constituent of OAM vortex beam generated by digital metasurface is comprehensively investigated. The phase quantization error of digital metasurface results in the loss of gain and aperture efficiency, which is quantitatively analyzed for different bit numbers. Fortunately, it is found that the OAM spectrum is barely affected by phase quantization, indicating that high purity OAM vortex beam can be generated by digital metasurface. Besides, the influence of topological charge l is also studied. It is observed that the growing of l will deteriorate the radiation performance of OAM vortex beam significantly and will stimulate dominant parasitic OAM modes at certain angle. Finally, the simulation and experiment of a 1-bit metasurface prototype demonstrate the numerical computations.

Acknowledgment

The authors thank Shan Jiang for valuable discussion.

References

[1] Allen L, Beijersbergen M W, Spreeuw R J C and Woerdman J P 1992 *Phys. Rev. A* **45** 8185
[2] Pu J X and Chen Z Y 2009 *Chin. Phys. Lett.* **26** 034202
[3] Zhao S M, Ding J, Dong X L and Zheng B Y 2011 *Chin. Phys. Lett.* **28** 124207
[4] Guo Z G and Yang G M 2017 *IEEE Antennas Wireless Propag. Lett.* **16** 404
[5] Cui X Z, Yin X L, Chang Huan, Zhang Z C, Wang Y J and Wu G H 2017 *Chin. Phys. B* **26** 114207
[6] Ji Z Y and Zhou G Q 2017 *Chin. Phys. B* **26** 094202
[7] Shen Y Z, Yang J W, Meng H F, Dou W B and Hu S M 2018 *Appl. Phys. Lett.* **112** 141901
[8] Thidé B, Then H, SjoHolm J, Palmer K, Bergman J, Carozzi T D, Istomin Y N, Ibragimov N H and Khamitova R 2007 *Phys. Rev. Lett.* **99** 087701
[9] Tamburini F, Mari E, Sponselli A, Thidé B, Bianchini A and Romanato F 2012 *New J. Phys.* **14** 033001
[10] Zhang C and Chen D 2017 *IEEE Antennas Wireless Propag. Lett.* **16** 2316
[11] Lin M, Gao Y, Liu P and Liu J 2016 *Electron. Lett.* **52** 1168
[12] Wei W L, Mahdjoubi K, Brousseau C and Emile O 2016 *IET Microw. Antennas Propag.* **10** 1420
[13] Mahmouli F E and Walker S D 2013 *IEEE Antennas Wireless Propag. Lett.* **2** 223
[14] Zhang Z F, Zheng S L, Jin X F, Chi H and Zhang X M 2016 *IEEE Antennas Wireless Propag. Lett.* **16** 8
[15] Yu S, Li L, Shi G, Zhu C, Zhou X and Shi Y 2016 *Appl. Phys. Lett.* **108** 121903
[16] Yu S, Li L, Shi G, Zhu C and Shi Y 2016 *Appl. Phys. Lett.* **108** 241901
[17] Yu S, Li L and Shi G 2016 *Appl. Phys. Express* **9** 082202

[18] Chen M L N, Jiang L J and Sha W E I 2018 *IEEE Antennas Wireless Propag. Lett.* **17** 110

[19] Zhang K, Yuan Y Y, Zhang D W, Ding X M, Ratni B, Burokur S N, Lu M J, Tang K and Wu Q 2018 *Opt. Express* **26** 1351

[20] Byun W J, Choi H D and Cho Y H 2017 *Sci. Rep.* **7** 12805

[21] Xu B J, Wu C, Wei Z Y, Fan Y C and Li H Q 2016 *Opt. Mater. Express* **6** 3940

[22] Giovampaola C D and Engheta N 2014 *Nat. Mater.* **13** 1115

[23] Yang H H, Yang F, Xu S H, Li M K, Cao X Y, Gao J and Zheng Y J 2017 *IEEE Antennas Wireless Propag. Lett.* **16** 302

[24] Zhao Y, Cao X Y, Gao J, Liu X and Li S J 2016 *Opt. Express* **24** 11208

[25] Yang H H, Yang F, Cao X Y, Xu S H, Gao J, Chen X B, Li M K and Li T 2017 *IEEE Trans. Antennas Propag.* **65** 3024

[26] Zhang D, Cao X Y, Yang H H, Gao J and Zhu X W 2018 *Opt. Express* **26** 24804

[27] Nayeri P, Yang F and Elsherbeni A Z 2013 *IEEE Antennas Propag. Magaine* **55** 127

[28] Meng X S, Wu J J, Wu Z S, Qu T and Yang L 2018 *Opt. Express* **26** 23185

[29] Lei X Y and Cheng Y J 2017 *IEEE Antennas Wireless Propag. Lett.* **16** 1357

[30] Jiang S, Chen C, Zhang H L and Chen W D 2018 *Opt. Express* **26** 6466

[31] Zhang D, Cao X Y, Yang H H and Gao J 2018 *IEEE Access* **6** 28691